Geophysical Research Letters

Supporting Information for

Global recharge dataset indicates strengthened groundwater connection to surface fluxes

Wouter R. Berghuijs[1], Elco Luijendijk[2, 5], Christian Moeck[3], Ype van der Velde[1], Scott T. Allen[4]

[1]Department of Earth Sciences, Free University Amsterdam, Amsterdam, Netherlands.

[2]Bundesgesellschaft für Endlagerung, Eschenstraße 55, 31224, Peine, Germany.

[3]Eawag - Swiss Federal Institute of Aquatic Science and Technology, Department Water Resources and Drinking Water, Dübendorf, Switzerland.

[4]Department of Natural Resources and Environmental Science, University of Nevada, Reno, Reno, USA.

[5]University of Bergen, Department of Earth Science, Allégaten 41, 5007, Bergen, Norway

Contents of this file

Introduction

This document contains several supplementary figures, a description of data used in these supplementary figures, and a test of the effects of our model parsimony.

Text S1. Additional site data

We also use 16 additional predictor variables collected by Moeck et al. (2020) for all groundwater recharge sites. These include mean precipitation (Fick & Hijmans, 2017), mean potential evapotranspiration (Trabucco & Zomer, 2009), temperature seasonality (Fick & Hijmans, 2017), precipitation seasonality (Fick & Hijmans, 2017) mean elevation (Danielson & Gesch, 2011), depth to water table (Fan et al., 2013), depth to bedrock (Wei et al., 2017), slope (Hengl et al., 2018a), topographic wetness index (Hengl et al., 2018b), the sand fraction, silt fraction, clay fraction, lithology, landform, land use (Friedl et al., 2010), and vegetation (FAPAR) (Hengl et al., 2018c). We refer to Moeck et al. (2020) and references therein for more information on these data.

Text S2. Model parsimony

The parsimony of this model (Eq. 1-2) could limit its predictive power, but making the model more complex does not substantially improve its predictive capacity. A split-sample test using 80% of the data for calibration and the remaining 20% for validation yields relatively narrow confidence bounds of the fitted parameters (95% confidence bounds α = 0.69 - 0.75, β = 14.0 - 16.2, not displayed), thus also subsets of the empirical data effectively constrain the relationship. The split-sample test also indicates the regional variation in groundwater recharge using Eq. 2 can be predicted with a much smaller bias (mean recharge bias = 8.9 mm·year^{-1}) than global hydrological models while explaining more of the site-to-site variability than most models (mean R^2 = 0.36; Fig. S4). Considering an additional 16 site attributes and a Neural Network fit with Levenberg-Marquardt optimization only slightly reduces the overall bias in the predictions (mean recharge bias = 7.9 mm·year^{-1}) and does not improve the explained site-to-site variability substantially (mean R^2 = 0.37; Fig. S3). Thus, compared to more complex methods, predictions of groundwater recharge based on climate aridity appear effective despite excluding many other factors that potentially also affect groundwater recharge. We, therefore, opted to use the most straightforward approach in our main paper.

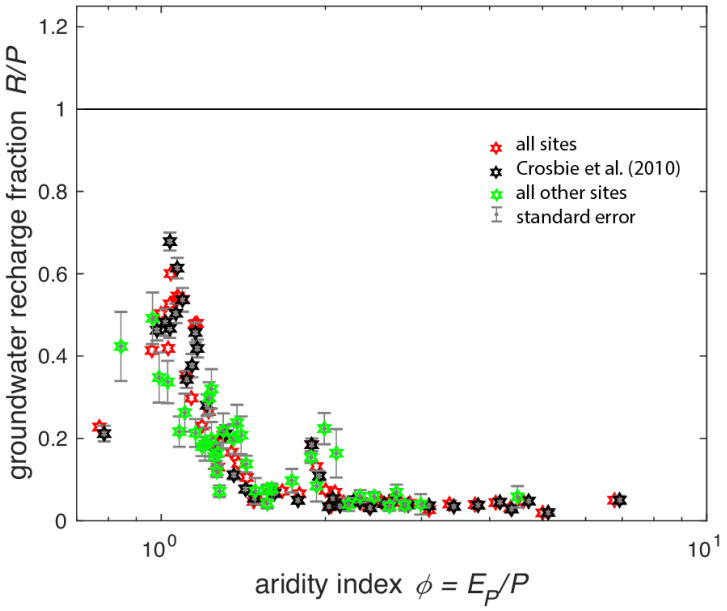

Figure S1. Relationship of aridity and recharge across subsets of the global observation-based recharge dataset. The recharge values are binned into 50 bins, each containing 2% of the data. The error bars display the standard error of the mean for each bin. These mean errors are larger for the recharge values not included in the Australian synthesis of Crosbie et al. (2010), because there are fewer data points included in per bin as there are fewer data points in the subset (n = 869 versus n = 4368).

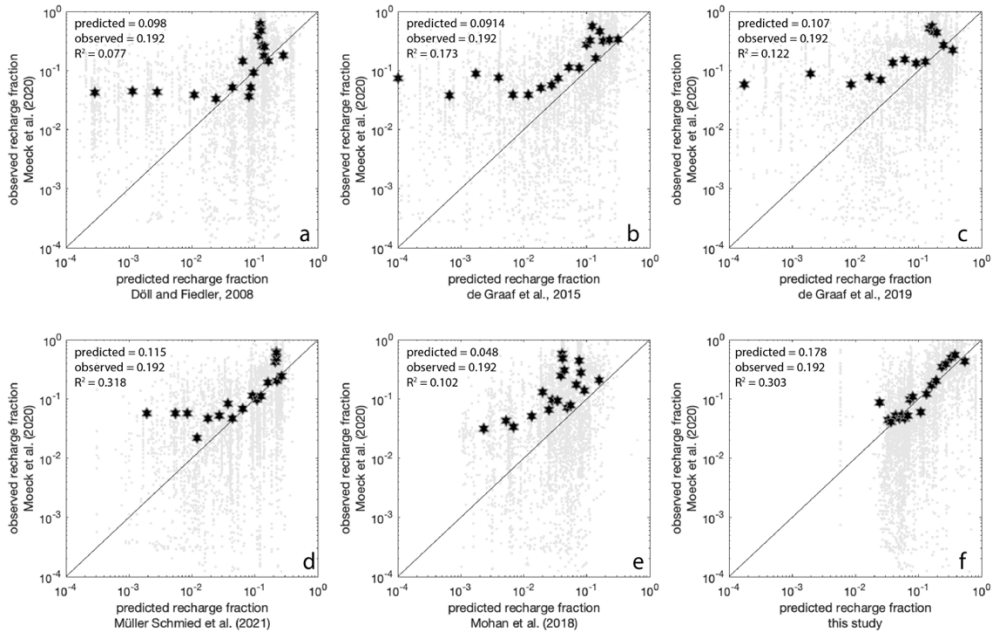

Figure S2. Recharge fractions in models and observations. Recharge fractions (the ratio of recharge to precipitation) at the 5327 observation sites are estimated with substantial biases by PCR-GLOB (**b**, **c**) WaterGAP (**a**, **d**) and machine learning compared to the simple aridity-recharge fraction relationship (this paper) (**f)**. The global hydrological models tend to underestimate the recharge fractions by over a factor of two for the observation sites. The recharge fractions are also binned into bins each containing 4% of the data. The recent version of WaterGAP (**d**) thereby slightly better simulates spatial differences in recharge rates than the simple aridity-recharge fraction relationship (this paper), but overall still has much lower recharge rates than the observation sites.

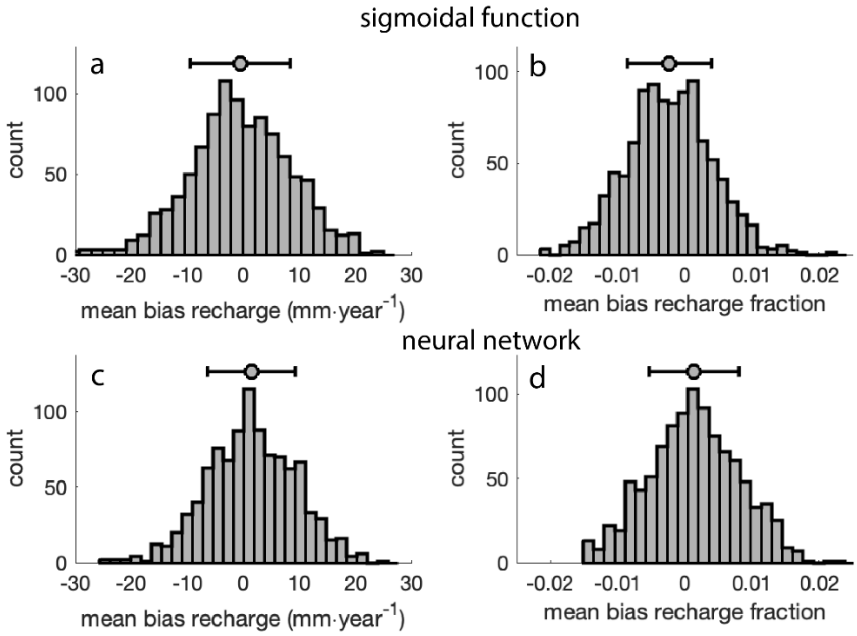

Figure S3. Mean error in predictions of groundwater recharge rates and recharge fractions at the validation sites. Histograms show the mean error in the prediction of groundwater recharge fractions (long-term recharge divided by long-term precipitation) using the sigmoidal function presented in this paper (**a**, **b**) and a neural network fitting approach (**c**, **d**) for 1000 repetitions of a split-sample test where 80% of the data from the 5237 recharge sites are used for calibration and the remaining 20% for validation. The marker indicates the mean of the values, and the whiskers indicate the standard deviation. These distributions indicate that models trained on several site properties may slightly outperform the sigmoidal function solely based on aridity, but differences are very small.

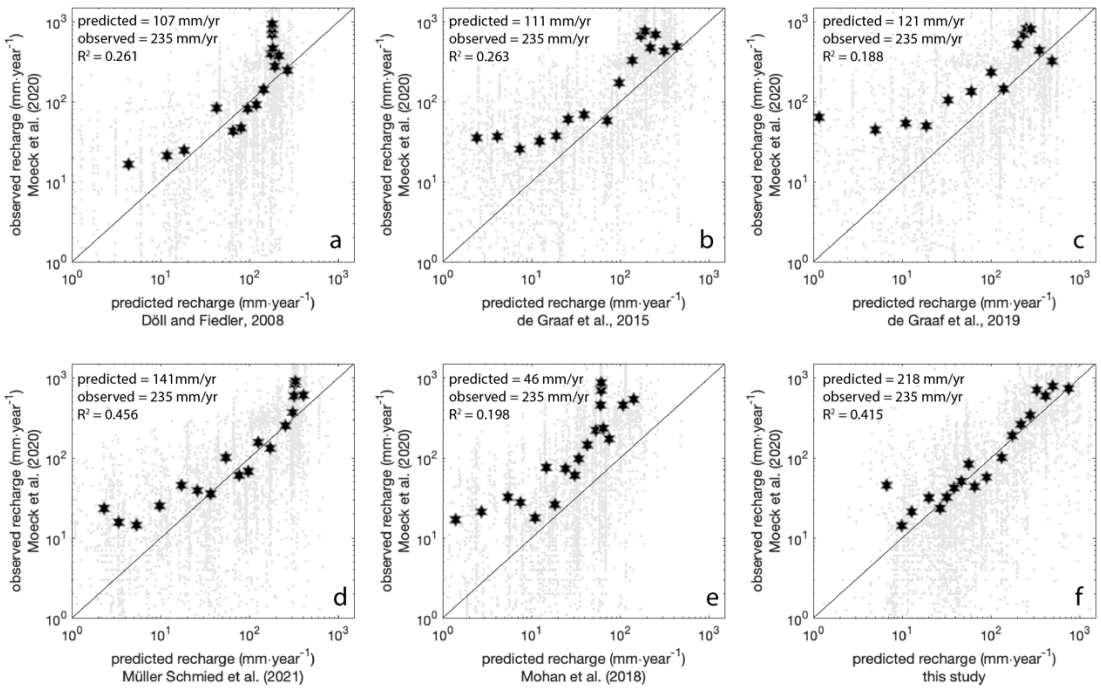

Figure S1. Comparison of predicted versus observed recharge for several global recharge predictions. Recharge predicted by global models such as PCR-GLOB, WATER-GAP, and machine learning (**a**-**e**) is systematically lower than recharge of the 5237 observation sites. The previous estimates (**a**-**e**) underestimate recharge by more than 50% compared to the recharge measurements. Using the sigmoid function (**f**) removes this bias and produces an overall average recharge of a very similar magnitude as global recharge estimates (**f**). The recharge rates are also binned into 25 bins for the plots, each containing 4% of the data.

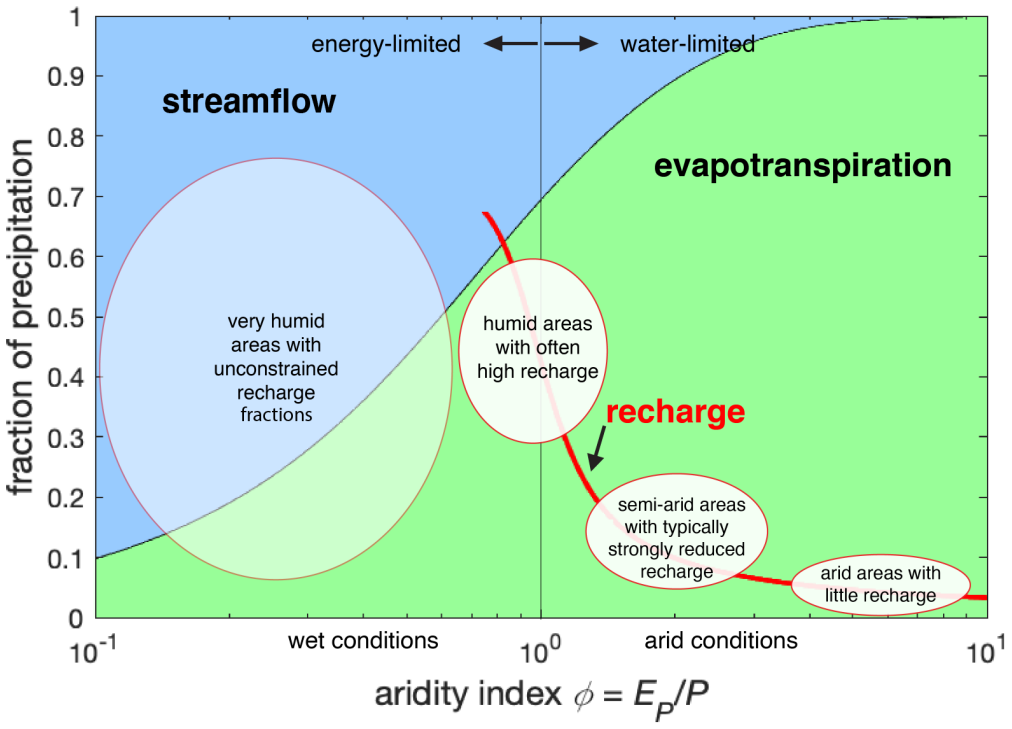

Figure S5. Conceptual representation of how groundwater recharge and its main fates vary with aridity. The partitioning of precipitation into streamflow and evapotranspiration follows the Budyko curve (Budyko, 1974). The redline is the aridity-recharge fraction relationship derived in this study presented in Fig. 1b.

References

Budyko, M. I. (1974). Climate and life (508 pp.). New York, NY: Academic Press.
Crosbie, R. S., Jolly, I. D., Leaney, F. W., & Petheram, C. (2010). Can the dataset of field based recharge estimates in Australia be used to predict recharge in data-poor areas?. Hydrology and Earth System Sciences, 14(10), 2023-2038.
Danielson, J.J., Gesch, D.B., (2011). Global Multi-resolution Terrain Elevation Data 2010 (GMTED2010). US Geological Survey.
Fan, Y., Li, H., & Miguez-Macho, G. (2013). Global patterns of groundwater table depth. Science, 339(6122), 940-943.
Fick, S. E. & Hijmans, R. J. (2017). WorldClim 2: new 1-km spatial resolution climate surfaces for global land areas. International Journal of Climatology. 37, 4302–4315.
Friedl, M.A., Sulla-Menashe, D., Tan, B., Schneider, A., Ramankutty, N., Sibley, A., Huang, X., (2010). MODIS Collection 5 global land cover: algorithm refinements and characterization of new datasets. Remote Sensing of Environment. 114, 168–182.
Hengl, T., (2018a). Global DEM Derivatives at 250 m, 1 km and 2 km Based on the MERIT DEM (Version 1.0) ([Data set]. Zenodo doi:105281/zenodo1447210).
Hengl, T., (2018b). Global Landform and Lithology Class at 250 m Based on the USGS Global Ecosystem Map (Version 1.0) ([Data set]. Zenodo doi:105281/zenodo1464846).
Hengl, T., (2018c) Fraction of Absorbed Photosynthetically Active Radiation (FAPAR) at 250m Monthly for Period 2014–2017 Based on COPERNICUS Land Products (Version 1.0) ([Data set]. Zenodo doi:105281/zenodo1450337).
Moeck, C., Grech-Cumbo, N., Podgorski, J., Bretzler, A., Gurdak, J. J., Berg, M., & Schirmer, M. (2020). A global-scale dataset of direct natural groundwater recharge rates: A review of variables, processes and relationships. Science of The Total Environment, 717, 137042.
Trabucco, A. & Zomer, R. J. Global Aridity and PET Database (CGIAR Consortium for Spatial Information, 2009); https://cgiarcsi.community/data/global-aridity-and-pet-database/
Wei, S.G., Hengl, T., de Jesus, J.M., Yuan, H., Dai, Y.J. (2017). Mapping the global depth to bedrock for land surface modeling. Journal of Advances in Modeling Earth Systems, 9, 65–88.
Yamazaki, D., Ikeshima, D., Tawatari, R., Yamaguchi, T., O'Loughlin, F., Neal, J.C., Sampson, C.C., Kanae, S., Bates, P. D. (2017). A high-accuracy map of global terrain elevations. Geophysical Research Letters, 44, 5844–5853.